Supporting Information

Catalysis at the rim: A mechanism for low temperature CO oxidation over Pt_3Sn

Matthias Vandichel,* Alina Moscu, and Henrik Grönbeck*

Department of Physics and Competence Centre for Catalysis, Chalmers University of Technology, 412 58 Göteborg, Sweden

To whom correspondence should be addressed: matvan@chalmers.se, ghj@chalmers.se

Table of contents

Optimized bulk structures and electronic energies

Table S1: Overview of the crystallographic cell parameters of the bulk structures with their space group Volume V ($Å^3$), bulkmodulus B (GPa), symmetry group, reference; in every cell the crystal angles are 90 ^{o} ($\alpha = \beta = \gamma = 90.0\ ^o$).

	a = b = c (Å)	Space/ group	V ($Å^3$)	B (GPa)	Symm. Group	Ref.
Pt	3.92	225	60.42		Fm-3m	Exp.
Pt	3.97	225	62.44	250	Fm-3m	This work
Sn	6.49	227	273.51		Fd-3m	Exp.
Sn	6.65	227	294.32	36	Fd-3m	This work
Pt_3Sn	4.00	221	64.00		Pm-3m	Exp.[1]
Pt_3Sn	4.06	221	66.78	200	Pm-3m	This work

	a (Å)	b (Å)	c (Å)	Space/ group	V ($Å^3$)	B (GPa)	Symm. Group	Ref.
SnO_2	4.74	4.74	3.19	136	71.51		P42/mnm	Exp.
SnO_2	4.82	4.82	3.24	136	75.50	183	P42/mnm	This work
SnO	3.80	3.80	4.82	129	69.40		P4/nmm	Exp.
SnO	3.87	3.87	4.91	129	73.70	45	P4/nmm	This work

Table S2: Overview of reaction energies ΔE_r between bulk phases (in eV).

	ΔE_r
$Sn + O_2 \rightarrow SnO_2$	-5.04
$Sn + 0.5O_2 \rightarrow SnO$	-2.65
$2Pt + 2Sn \rightarrow Pt_2Sn_2$	-2.34
$3Pt + Sn \rightarrow Pt_3Sn$	-1.53
$Pt_3Sn \rightarrow 2Pt + PtSn$	0.36
$Pt_3Sn + 0.5O_2 \rightarrow 3Pt + SnO$	-1.13
$Pt_3Sn + O_2 \rightarrow 3Pt + SnO_2$	-3.51
$PtSn + 0.5O_2 \rightarrow Pt + SnO$	-1.49
$PtSn + O_2 \rightarrow Pt + SnO_2$	-3.87

Ab Initio Thermodynamics of the segregation process

Schematic representation of partial segregation

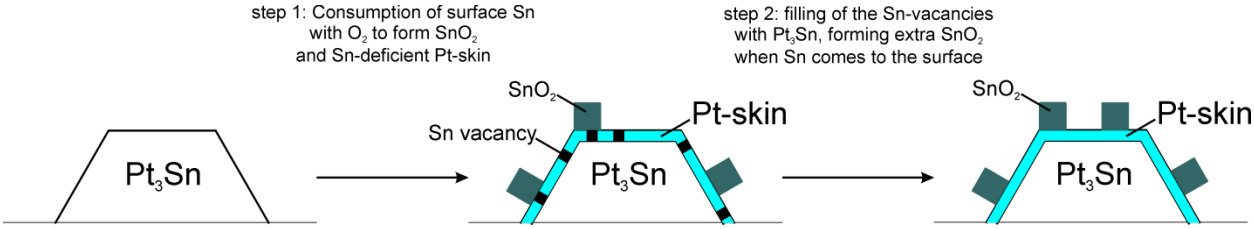

Figure S1: Schematic representation of the formation of a Pt-skin during surface segregation of a Pt_3Sn nanoparticle

Adsorption energies for CO and O on $Pt_3Sn(111)$ and $Pt(111)/Pt_3Sn$

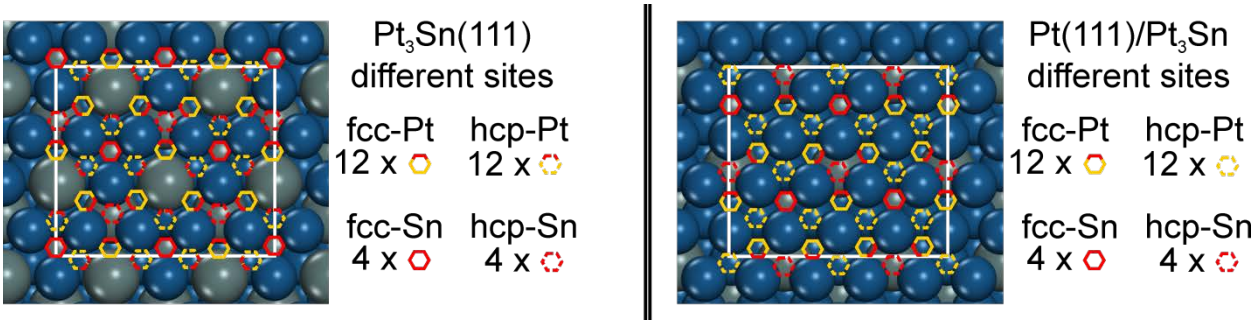

Figure S2: Different possible adsorbate positions within $Pt_3Sn(111)$ and $Pt(111)/Pt_3Sn$ unit cells. Fcc adsorption sites (full hexagons), hcp-adsorption sites (dotted hexagons). Hexagons are colored based on the atoms in the second layer for fcc sites and first layer for hcp sites, with colorcodes (Pt, yellow) and (Sn, red).

Table S3: Adsorption energies of CO (1/16 ML) and O (1/16 ML) on different adsorption positions of Pt(111), Pt_3Sn(111) and Pt(111)/Pt_3Sn

Adsorbate	**Pt(111)**			
	position	ΔE_{ads}		
CO	H_{Pt3} hcp-Pt	-1.91		
CO	H_{Pt3} fcc-Pt	-1.87		
O	H_{Pt3} hcp-Pt	-0.89		
O	H_{Pt3} fcc-Pt	-1.27		
	Pt_3Sn(111)		**Pt(111)/Pt_3Sn**	
	position	ΔE_{ads}	position	ΔE_{ads}
CO	H_{Pt2Sn} hcp-Pt → Pt_2-bridge	-1.38	H_{Pt3} hcp-Pt	-1.98
CO	H_{Pt3} hcp-Sn	-1.95	H_{Pt3} hcp-Sn	-1.96
CO	H_{Pt2Sn} fcc-Pt → Pt_2-bridge	-1.88	H_{Pt3} fcc-Pt	-2.08
CO	H_{Pt3} fcc-Sn	-1.49	H_{Pt3} fcc-Sn	-1.59
O	H_{Pt2Sn} hcp-Pt	-0.81	H_{Pt3} hcp-Pt	-1.07
O	H_{Pt3} hcp-Sn	-0.82	H_{Pt3} hcp-Sn	-0.82
O	H_{Pt2Sn} fcc-Pt	-1.28	H_{Pt3} fcc-Pt	-1.36
O	H_{Pt3} fcc-Sn	-0.42	H_{Pt3} fcc-Sn	-1.12

Table S4: Average adsorption energies of CO (1/4 ML) and O (1/4 ML) on different adsorption positions of Pt(111), Pt_3Sn(111) and Pt(111)/Pt_3Sn. Results determined in a unit-cell with 4x4 surface atoms.

	positions	ΔE_{ads}
Pt(111)		
CO	H_{Pt3} hcp-Pt	-1.80
O	H_{Pt3} fcc-Pt	-1.25
Pt_3Sn(111)		
CO	H_{Pt3} hcp-Sn	-1.64
O	H_{Pt2Sn} fcc-Pt	-1.14
Pt(111)/Pt_3Sn		
CO	H_{Pt3} fcc-Pt	-1.92
O	H_{Pt3} fcc-Pt	-1.40

Applied computational methodology for the phase diagram construction

Here we elaborate on equation 1 and 2 (see main text). In these equations, we approximated the chemical potentials μ for bulk and surfaces by the internal energy E:

$$G = E + PV - TS \approx E$$

For surface slabs and bulk structures, the PV term can be neglected for the rather low pressures under consideration here as well as the TS term, which includes the entropy contributions.

To evaluate equation 2 of the main text for different phases, the chemical potentials for CO and oxygen have to be expressed in function of temperature and pressure;

$$\mu_O\,(T,p) = \tfrac{1}{2}E_{O_2}^{tot} + \Delta\mu_O(T,p) = \tfrac{1}{2}E_{O_2}^{tot} + \Delta\mu_O(T,p^0) + \tfrac{1}{2}k_B T.\ln(\tfrac{p_{O_2}}{p^0})$$

$$\mu_{CO}(T,p) = E_{CO}^{tot} + \Delta\mu_{CO}(T,p) = E_{CO}^{tot} + \Delta\mu_{CO}(T,p^0) + k_B T.\ln(\frac{p_{CO}}{p^0})$$

Here, $E_{O_2}^{tot}$ and E_{CO}^{tot} represent the zero-point corrected energies. Based on equation 2 (main text), the different phases can be analyzed as a function of $\Delta\mu_O(T,p)$ and $\Delta\mu_{CO}(T,p)$ (**Figure 1**). Moreover, using the tabulated standard chemical potentials $\Delta\mu(T,p^0)$ at $p^0 = 1$ bar [2], a pressure axis can be constructed for any given temperatures (**Figures S3**).

The standard chemical potentials $\Delta\mu(T,p^0)$ at $p^0 = 1$ bar can be calculated from enthalpy and entropy; for example $\Delta\mu_O(T,p^0) = \frac{1}{2}\big(H(T,p^0,O_2) - H(0\ K,p^0,O_2)\big) - \frac{1}{2}.T.\,(S(T,p^0,O_2) - S(0\ K,p^0,O_2))$ and similarly for $\Delta\mu_{CO}(T,p^0) = \big(H(T,p^0,CO) - H(0\ K,p^0,CO)\big) - T.\,(S(T,p^0,CO) - S(0\ K,p^0,CO))$.

Phase diagram at different temperatures

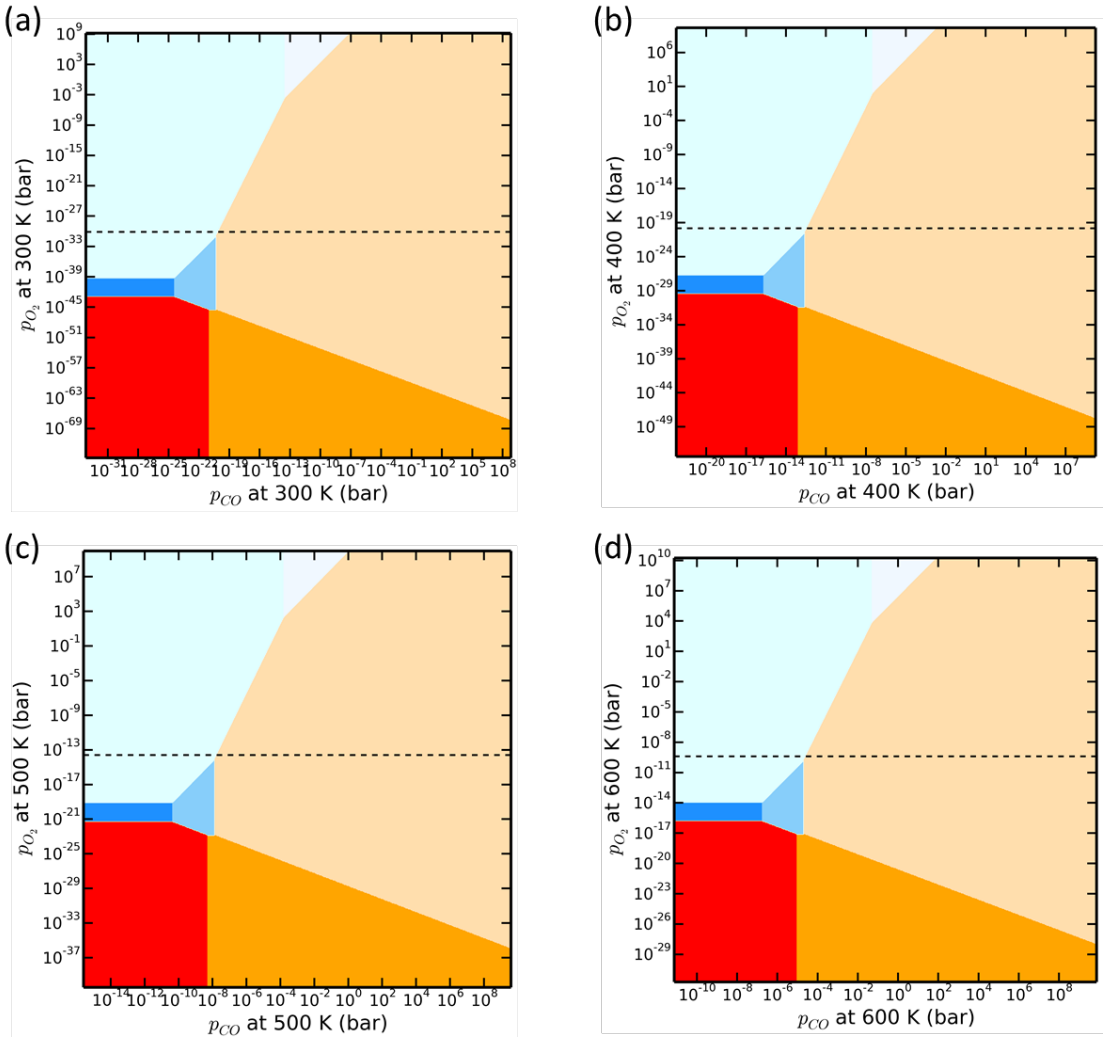

Figure S3: Phase diagrams with pressure scales at different temperatures, see main text for the assignation of the surfaces; (a) 300 K, (b) 400 K, (c) 500 K and (d) 600 K. Dotted line indicates from which oxygen pressure the transition towards our SnO_2/Pt-skin model (see Figure 2b and 2c in main text) becomes thermodynamically favorable.

Reaction barriers for CO oxidation on metal-sites, FAR and CLOSE to the SnO_2 rod

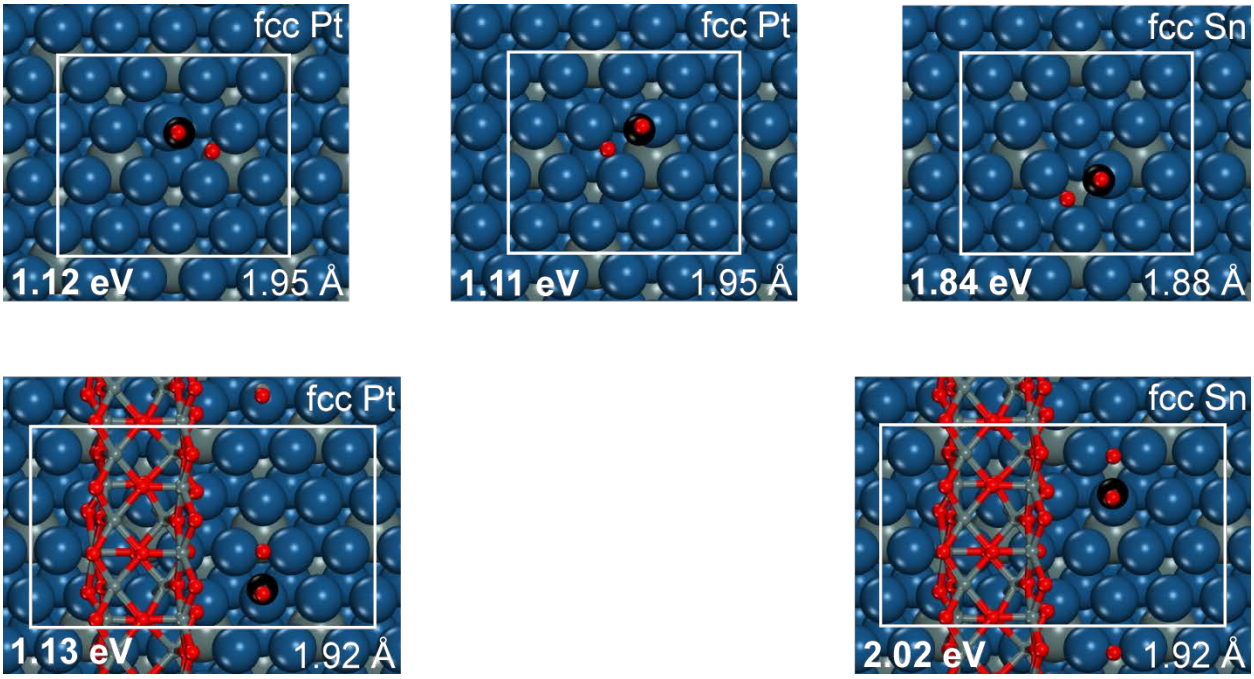

Figure S4: Representation of transitions states FAR and CLOSE to the SnO_2-rod (Pt-skin system). The reaction barriers (from CO and O adsorbed in their most stable positions within separate unit cells) and O—CO distances are shown.

Mean Field Microkinetic model

Construction of a molecular model for the description of CO-oxidation on a SnO_x/Pt interface

To assess whether or not it is feasible to construct a fully periodic system, the unit cell dimensions of SnO_2 and Pt are compared according with their most favorable exposed surface (lowest surface energy). These are the 110 and 111 surface for SnO_2 and Pt respectively (**Figure S5**). SnO_2 rods with each 12 Sn atoms and 24 oxygen atoms (with 4 times the (110) as exposed surface) were placed differently on top of Pt(111) (full segregation) and Pt(111)/Pt_3Sn(111) (as shown for a SnO_2/Pt(111)/Pt_3Sn model in **Figure S6**).

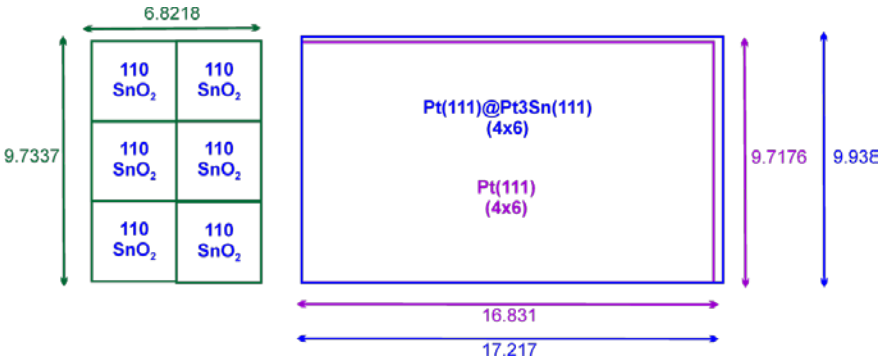

Figure S5: Matching the unit cells of SnO_2 (green), Pt(111) (purple) and Pt(111)/Pt_3Sn (blue)

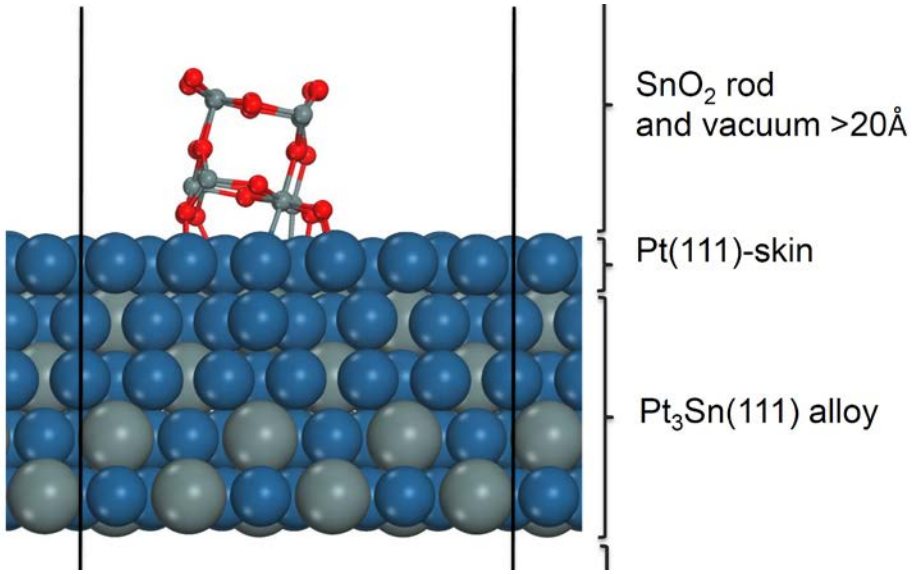

Figure S6: Sideview of the SnO_2/Pt interface system ; three of the four SnO_2(110) surfaces are exposed, one SnO_2(110) surface makes the connection with the Pt-skin supported by Pt_3Sn.

Some of the most stable amongst the optimized rods are presented (top view) in **Figure S7**. For the SnO_2-rods, we determined the charge transfer between the rod and the metal slab (**Table S5**). The adsorption energy of the SnO_2 rod with respect to the SnO_2 bulk was also determined (**Table S6**). As the adsorption energies seem rather endothermic with the SnO_2 bulk as reference, we decided to use the most stable **SnO_2/Pt(111)/Pt_3Sn** system (**Figure S7**) and investigate the impact on the adsorption energies and charge transfer.

The transfer of charge from the slab to the rod $(SnO_2)_{12}$, is about 0.8 electrons for the skin system and a bit less for SnO_2/Pt(111) (0.6e) (see **Table S5**). To determine the adsorption energy of the rod onto the metal, both the $(SnO_2)_{12}$-rod and the metal slab were optimized separately in the same unit cell. The adsorption energy of the $(SnO_2)_{12}$-rod onto the $(6 \times 2\sqrt{3})_{rect}$ skin system amounts to about -4.5 eV.

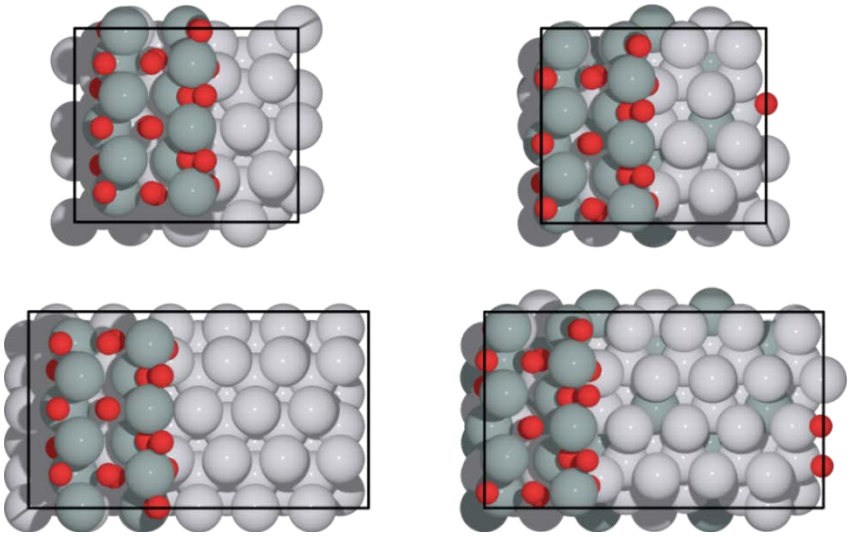

Figure S7: Calculated SnO_2-rod on Pt(111) (4Layers, 2x2x1 k-point grid, 450 eV) and SnO_2 rod on Pt@Pt_3Sn(111) (1 Layer Pt, 4Layers Pt_3Sn, k-point grids of respectively 2x2x1 and 2x3x1, energy cut off of 450 eV). Metal slab geometries $(4 \times 2\sqrt{3})_{rect}$ and $(6 \times 2\sqrt{3})_{rect}$.

Table S5: Charge transfer from the SnO_2 rod to the metal slab, determined via Bader analysis (600 eV, 3x3x1 k-point grid for $(4 \times 2\sqrt{3})$rect, and 2x3x1 k-point grid for $(6 \times 2\sqrt{3})$rect). Positive values indicate the charge of the metal slab that is transferred to the SnO_2 rod.

	metal slab geometry	
	$(4 \times 2\sqrt{3})$rect	$(6 \times 2\sqrt{3})$rect
Charge transfer	3x3x1, 600 eV	2x3x1, 600 eV
SnO_2/Pt(111)	+0.615e	-
SnO_2/Pt/Pt_3Sn(111)	+0.798e	+0.763e

Table S6: Adsorption energies (in eV) of the SnO_2 rod on the metal slab with respect to SnO_2 in the bulk phase

	metal slab geometry	
	(4 x $2\sqrt{3}$)rect	(6 x $2\sqrt{3}$)rect
Adsorption energy	3x3x1, 600 eV	2x3x1, 600 eV
SnO_2/Pt(111)	9.82	
SnO_2/Pt(111)/Pt_3Sn	8.68	
Adsorption energy	2x2x1, 450 eV	2x3x1, 450 eV
SnO_2/Pt(111)	9.77	
SnO_2/Pt(111)/Pt_3Sn	8.78	

To investigate the exothermicity of the segregation hypothesis, we can consider the following reaction from a 5 layer Pt_3Sn slab. Assume that we start from a (9 x $2\sqrt{3}$)rect unit cell and three bulk units of Pt_3Sn. In this case, 9 surface Sn atoms and 3 Sn atoms (Pt_3Sn bulk) can form the $(SnO_2)_{12}$-rod. The reaction energy for segregation is calculated as follows:

E[Pt(111)/Pt_3Sn-slab, (3 x $2\sqrt{3}$)$_{rect}$] + E[$(SnO_2)_{12}$/Pt(111)/Pt_3Sn-slab, (6 x $2\sqrt{3}$)$_{rect}$] – (E[Pt_3Sn-slab, (9 x $2\sqrt{3}$)$_{rect}$] + 3E[Pt_3Sn-bulk] + 12(E[O_2] + $2.\Delta\mu_O$)), with a reaction energy of -27.06 eV (-28.10 eV if zero-point corrected energy for O_2 is used). This is about -2.25 eV per SnO_2 unit. If we form bulk SnO_2 instead of a rod, we would obtain a reaction energy of -35.75 eV (-36.80 eV if zero-point corrected energy for O_2 is used). This reaction to the bulk is thus even a more exothermic by -0.72 eV per SnO_2 unit formed. In total that is about -2.97 eV per SnO_2 formed. Although it is thermodynamically feasible to create a metal supported SnO_2 phase, we cannot predict at which temperatures this transformation becomes kinetically favorable. In experiment, one has to increase the temperatures above 473 K, to see the appearance of these SnO_2 phases from Pt_3Sn(111) at 500 mTorr O_2.[3]

Within the constructed phase diagram **(Figure 1** and **Figure S3**), we use formula 2 (eq.2 in main text) to compare different surfaces with 12 surface atoms. Here, the formation of SnO_2, leads to a stabilization of -3.2 eV per bulk SnO_2-unit if $N_O = N_{CO} = 0$. This is an over-estimation, so in practice, the segregation line in Figure 1, should be expected to lie at higher $\Delta\mu_O$.

Construction of the mean-field Microkinetic Model (MF-MKM)

The site distribution

In the mean field micro-kinetic model (MF-MKM), three types of sites are considered (FAR, CLOSE and SnO_2). The sites in the interphase region between the Pt-skin (FAR-sites) and the oxide (SnO_2-sites) are defined as sites of type CLOSE. In other words, these interphase sites are close to the FAR-sites as well as the SnO_2 sites as indicated in the very rudimentary schematic representation below (**Figure S8**).

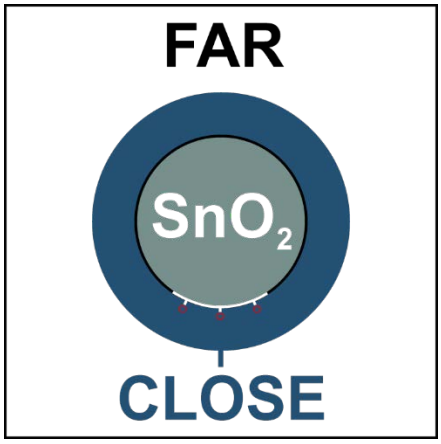

Figure S8: Distribution of the sites in the MF-MKM on a propotional scale.

To find a good site distribution within the MKM, the following reasoning was made:

- Take an average Pt_3Sn-NP of 4 nm in diameter. The exposed surface of this hemispheric NP can be projected onto a square of 25 nm^2
- Assume the existence of a spherical SnO_2 – phase formed after segregation of about 2nm diameter on this square; and around this SnO_2 –unit, there is an interphase region of ~0.5 nm (CLOSE sites). CO adsorbed on the CLOSE sites can directly react with the SnO_2 rod.
- The site distribution is then as follows; 12% SnO_2-sites, 16% CLOSE-sites and 72% FAR-sites

Reaction steps in the ab initio mean-field microkinetic model

For the CO oxidation on Pt(111) or the Pt(111)/Pt_3Sn(111) system, there are already many existing microkinetic models based on the conventional Langmuir-Hinshelwood mechanism where the competitive CO and O_2 adsorption processes occur associatively and dissociatively, [4-5]:

$CO + * \leftrightarrow CO*$	(**R1**) for FAR and CLOSE-sites
$O_2 + 2* \leftrightarrow 2O*$	(**R2**) for FAR and CLOSE-sites
$[O,CO]* \leftrightarrow O\text{-}CO^{*,TS} \leftrightarrow CO_2(g) + 2*$	(**R3**) for FAR and CLOSE-sites
$CO* + SnO_2 \leftrightarrow CO_2(g) + SnO$	(**R4**) for CLOSE/SnO_2 interphase

The * denotes a free surface site and X* an adsorbate X bonded to a surface site. Remark that after CO oxidation, the produced CO_2 goes directly to the gas phase. We assume that CO adsorption can happen on sites of type FAR or CLOSE, while O_2 adsorption can happen on each of the three types of sites (FAR, CLOSE, SnO_2). The CO-oxidation happens on FAR or CLOSE sites and between CO on close sites and oxygen atoms of the SnO_2 rod that are in contact with the Pt-skin. For site type SnO_2, $N = 8$ different structures with different degree of oxygenation are considered and named $\theta^i_{SnO_2}$ (*Si in Figure S9). A more detailed overview of all included reaction steps is given in Table 1 of the main paper.

For each type of site (FAR, CLOSE, SnO_2), we can thus write a site balance:

$$\theta^*_{FAR} = FAR - \theta^{CO}_{FAR} - \theta^{O}_{FAR}$$

$$\theta^*_{CLOSE} = CLOSE - \theta^{CO}_{CLOSE} - \theta^{O}_{CLOSE}$$

$$SnO_2 = \sum_{i=0}^{N} \theta^i_{SnO_2}$$

For conciseness, the different SnO_X-phases are indicated with numbers from 1 til 8 within the following differential equations. To compare with the triletter code used in the main paper, we refer the reader to **Figure S9**.

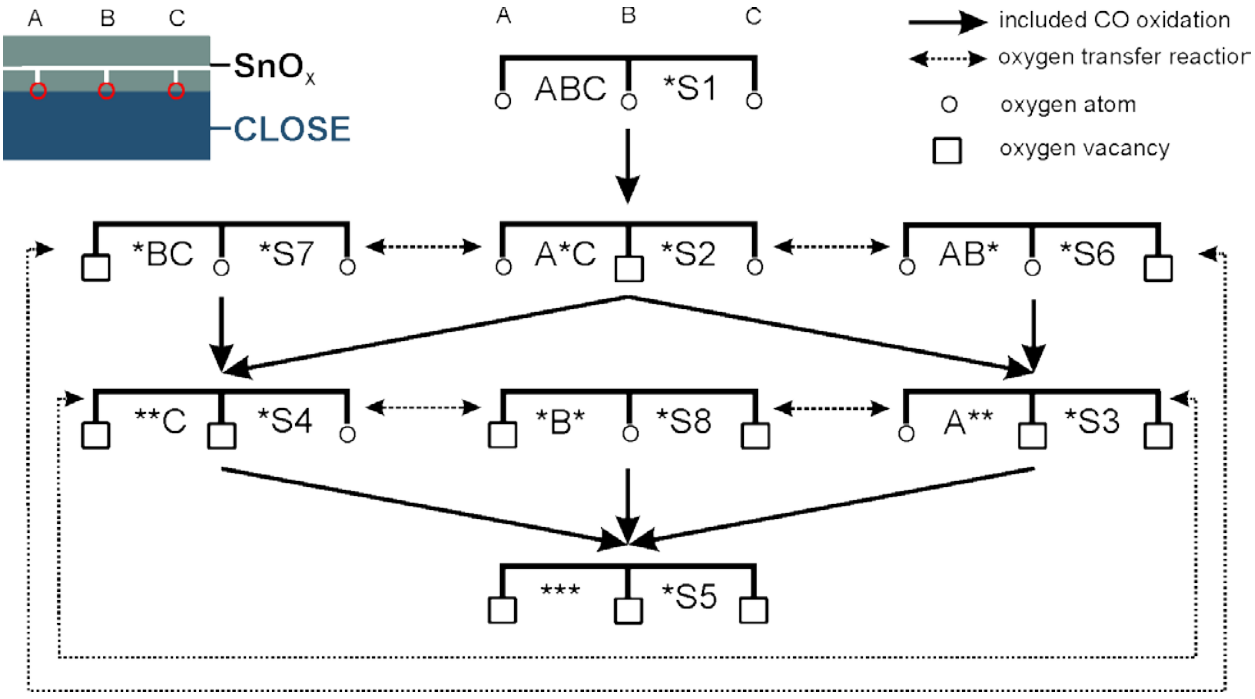

Figure S9. Schematic overview of the nomenclature used for the different SnO_X states.

Differential equations

The corresponding equations **(1-4)** on FAR and CLOSE sites are:

$$\frac{d\theta_{FAR}^{CO}}{dt} = R_{ads}^{CO}.\theta_{FAR}^{*} - \frac{R_{ads}^{CO}}{\left(K_{ads,FAR}^{CO}.\frac{p_{CO}}{R.T}\right)}\theta_{FAR}^{CO}$$
$$-k_{fwd,FAR}.(\theta_{FAR}^{CO}\theta_{FAR}^{O}) + k_{bwd,FAR}.\left(K_{ads}^{CO_2}.\frac{p_{CO_2}}{R.T}\right).(\theta_{FAR}^{*})^2$$

(DV-1)

$$\frac{d\theta_{FAR}^{O}}{dt} = 2.R_{ads}^{O_2}.(\theta_{FAR}^{*})^2 - 2.\frac{R_{ads}^{O_2}}{\left(K_{ads,FAR}^{O_2}.\frac{p_{O_2}}{R.T}\right)}.(\theta_{FAR}^{O})^2$$
$$-k_{fwd,FAR}.(\theta_{FAR}^{CO}\theta_{FAR}^{O}) + k_{bwd,FAR}.\left(K_{ads,FAR}^{CO_2}.\frac{p_{CO_2}}{R.T}\right).(\theta_{FAR}^{*})^2$$

(DV-2)

$$\frac{d\theta_{CLOSE}^{CO}}{dt} = R_{ads}^{CO}.\theta_{CLOSE}^{*} - \frac{R_{ads}^{CO}}{\left(K_{ads,CLOSE}^{CO}.\frac{p_{CO}}{R.T}\right)}\theta_{CLOSE}^{CO}$$
$$-k_{fwd,CLOSE}.(\theta_{CLOSE}^{CO}\theta_{CLOSE}^{O}) + k_{bwd,CLOSE}.\left(K_{ads,CLOSE}^{CO_2}.\frac{p_{CO_2}}{R.T}\right).(\theta_{CLOSE}^{*})^2$$
$$-k_{fwd,1\to2}.\left(\theta_{CLOSE}^{CO}\theta_{SnO_2}^{1}\right) + k_{bwd,1\to2}.\left(K_{ads,1\to2}^{CO_2}.\frac{p_{CO_2}}{R.T}\right).(\theta_{CLOSE}^{*}).(\theta_{SnO_2}^{2})$$
$$-k_{fwd,2\to3}.\left(\theta_{CLOSE}^{CO}\theta_{SnO_2}^{2}\right) + k_{bwd,2\to3}.\left(K_{ads,2\to3}^{CO_2}.\frac{p_{CO_2}}{R.T}\right).(\theta_{CLOSE}^{*}).(\theta_{SnO_2}^{3})$$
$$-k_{fwd,2\to4}.\left(\theta_{CLOSE}^{CO}\theta_{SnO_2}^{2}\right) + k_{bwd,2\to4}.\left(K_{ads,2\to4}^{CO_2}.\frac{p_{CO_2}}{R.T}\right).(\theta_{CLOSE}^{*}).(\theta_{SnO_2}^{4})$$
$$-k_{fwd,3\to5}.\left(\theta_{CLOSE}^{CO}\theta_{SnO_2}^{3}\right) + k_{bwd,3\to5}.\left(K_{ads,3\to5}^{CO_2}.\frac{p_{CO_2}}{R.T}\right).(\theta_{CLOSE}^{*}).(\theta_{SnO_2}^{5})$$
$$-k_{fwd,4\to5}.\left(\theta_{CLOSE}^{CO}\theta_{SnO_2}^{4}\right) + k_{bwd,4\to5}.\left(K_{ads,4\to5}^{CO_2}.\frac{p_{CO_2}}{R.T}\right).(\theta_{CLOSE}^{*}).(\theta_{SnO_2}^{5})$$
$$-k_{fwd,6\to3}.\left(\theta_{CLOSE}^{CO}\theta_{SnO_2}^{6}\right) + k_{bwd,6\to3}.\left(K_{ads,6\to3}^{CO_2}.\frac{p_{CO_2}}{R.T}\right).(\theta_{CLOSE}^{*}).(\theta_{SnO_2}^{3})$$
$$-k_{fwd,7\to4}.\left(\theta_{CLOSE}^{CO}\theta_{SnO_2}^{7}\right) + k_{bwd,7\to4}.\left(K_{ads,7\to4}^{CO_2}.\frac{p_{CO_2}}{R.T}\right).(\theta_{CLOSE}^{*}).(\theta_{SnO_2}^{4})$$
$$-k_{fwd,8\to5}.\left(\theta_{CLOSE}^{CO}\theta_{SnO_2}^{8}\right) + k_{bwd,8\to5}.\left(K_{ads,8\to5}^{CO_2}.\frac{p_{CO_2}}{R.T}\right).(\theta_{CLOSE}^{*}).(\theta_{SnO_2}^{5})$$

(DV-3)

$$\frac{d\theta^{O}_{CLOSE}}{dt} = 2.R^{O_2}_{ads}.\left(\theta^{*}_{CLOSE}\right)^2 - 2.\frac{R^{O_2}_{ads}}{\left(K^{O_2}_{ads,FAR}.\frac{p_{O_2}}{R.T}\right)}.\left(\theta^{O}_{CLOSE}\right)^2$$
$$-k_{fwd,CLOSE}.\left(\theta^{CO}_{CLOSE}\theta^{O}_{CLOSE}\right) + k_{bwd,CLOSE}.\left(K^{CO_2}_{ads,CLOSE}.\frac{p_{CO_2}}{R.T}\right).\left(\theta^{*}_{CLOSE}\right)^2$$

(DV-4)

In which, $\theta^{species}_{phase}$ represents the coverages of a certain species on a certain phase; p_{CO_2}, p_{CO} and p_{O_2} are the pressures.

Furthermore, the rate coefficients for CO oxidation [1/s] are indicated as k,

$$k_{fwd,phase} = \frac{q^{TS}}{q^{R}}\exp(-\frac{\Delta H^{R\to TS}}{RT}),\ k_{bwd,phase} = \frac{q^{TS}}{q^{P}}\exp(-\frac{\Delta H^{P\to TS}}{RT})$$

Which contains the vibrational partition function of transition state and reactant state, q^{TS} and q^{R} respectively. The activation barriers for the CO oxidation reaction and the backward CO_2 dissociation reaction are not scaled by the coverage of CO and O.

With R^{GAS}_{ads}, the rate of adsorption for a GAS (CO, O_2, CO_2), when multiplied by an empty site coverage.

$$R^{GAS}_{ads} = \frac{s^{GAS}_{phase}.N_A.A^{site}.p_{GAS}}{\sqrt{2\pi.m_{GAS}.R.T}}$$

Here, s^{GAS}_{phase} represents the sticking coefficient [-], A^{site} the surface of one site [m^2], N_A Avogadro`s number [1/mol], p_{GAS} the pressure, m_{GAS} the molar mass [kg/mol], R the universal gas constant for an ideal gas [J/mol/K] and T the temperature [K].

The rate of desorption of a species (O, CO) is given by R^{GAS}_{des} [1/s], which is computed from R^{GAS}_{ads} divided by the equilibrium constant for adsorption of the GAS, $K^{GAS}_{ads,phase}$[m^3/mol] (GAS + * ↔ GAS*):

$$R^{GAS}_{des} = \frac{R^{GAS}_{ads}}{K^{GAS}_{ads,phase}.(\frac{p_{GAS}}{R.T})}$$

With an equilibrium constant $K^{GAS}_{ads,phase}$ defined as follows;

$$K^{GAS}_{ads,phase} = \frac{q^{GAS^*}}{q^{*}.q^{GAS}}\exp(-\frac{\Delta H^{GAS}_{ads}(1-f)}{RT})$$

In which q^{GAS} represents the global function containing translations, rotations and vibrations [mol/m^3], $q^{GAS} = q_{trans}.q_{rot}.q_{vib}$. Dependent on which gas adsorbs, a term correcting for the CO an O repulsions is included $f_{ads=O2} = \alpha.\frac{\theta^{O}_{phase}}{phase}, f_{ads=CO} = \beta.\frac{\theta^{CO}_{phase}}{phase}$ (see below).

The SnO_2 phase can interact only with species on CLOSE sites. For the SnO_2-phase, we abbreviated the 8 states of the SnO_2-rod (as defined in Scheme 1) with numbers from 1 to 8: ABC (1), A*C (2), A** (3), **C (4), *** (5), AB* (6), *BC (7) and *B* (8) . The rate equations are written below:

$$\frac{d\theta^1_{SnO_2}}{dt} = -k_{fwd,1\to2}.\left(\theta^{CO}_{CLOSE}\theta^1_{SnO_2}\right) + k_{bwd,1\to2}.\left(K^{CO_2}_{ads,1\to2}.\frac{p_{CO_2}}{R.T}\right).(\theta^*_{CLOSE}).(\theta^2_{SnO_2})$$
$$+R^{O_2}_{ads}.\theta^3_{SnO_2} - \frac{R^{O_2}_{ads}}{\left(K^{O_2}_{ads,SnO_2,3\to1}.\frac{p_{O_2}}{R.T}\right)}.\theta^1_{SnO_2}$$
$$+R^{O_2}_{ads}.\theta^4_{SnO_2} - \frac{R^{O_2}_{ads}}{\left(K^{O_2}_{ads,SnO_2,4\to1}.\frac{p_{O_2}}{R.T}\right)}.\theta^1_{SnO_2}$$
$$+R^{O_2}_{ads}.\theta^8_{SnO_2} - \frac{R^{O_2}_{ads}}{\left(K^{O_2}_{ads,SnO_2,8\to1}.\frac{p_{O_2}}{R.T}\right)}.\theta^1_{SnO_2}$$

(DV-5)

$$\frac{d\theta^2_{SnO_2}}{dt} = k_{fwd,1\to2}.\left(\theta^{CO}_{CLOSE}\theta^1_{SnO_2}\right) - k_{bwd,1\to2}.\left(K^{CO_2}_{ads,1\to2}.\frac{p_{CO_2}}{R.T}\right).(\theta^*_{CLOSE}).(\theta^2_{SnO_2})$$
$$-k_{fwd,2\to3}.\left(\theta^{CO}_{CLOSE}\theta^2_{SnO_2}\right) + k_{bwd,2\to3}.\left(K^{CO_2}_{ads,2\to3}.\frac{p_{CO_2}}{R.T}\right).(\theta^*_{CLOSE}).(\theta^3_{SnO_2})$$
$$-k_{fwd,2\to4}.\left(\theta^{CO}_{CLOSE}\theta^2_{SnO_2}\right) + k_{bwd,2\to4}.\left(K^{CO_2}_{ads,2\to4}.\frac{p_{CO_2}}{R.T}\right).(\theta^*_{CLOSE}).(\theta^4_{SnO_2})$$
$$+R^{O_2}_{ads}.\theta^5_{SnO_2} - \frac{R^{O_2}_{ads}}{\left(K^{O_2}_{ads,SnO_2,5\to2}.\frac{p_{O_2}}{R.T}\right)}.\theta^2_{SnO_2}$$
$$-k_{fwd,O-transfer,2\to6}.\theta^2_{SnO_2} + k_{bwd,O-transfer,2\to6}.\theta^6_{SnO_2}$$
$$-k_{fwd,O-transfer,2\to7}.\theta^2_{SnO_2} + k_{bwd,O-transfer,2\to7}.\theta^7_{SnO_2}$$

(DV-6)

$$\frac{d\theta^3_{SnO_2}}{dt} = k_{fwd,2\to3}.\left(\theta^{CO}_{CLOSE}\theta^2_{SnO_2}\right) - k_{bwd,2\to3}.\left(K^{CO_2}_{ads,2\to3}.\frac{p_{CO_2}}{R.T}\right).(\theta^*_{CLOSE}).(\theta^3_{SnO_2})$$
$$+k_{fwd,6\to3}.\left(\theta^{CO}_{CLOSE}\theta^6_{SnO_2}\right) - k_{bwd,6\to3}.\left(K^{CO_2}_{ads,6\to3}.\frac{p_{CO_2}}{R.T}\right).(\theta^*_{CLOSE}).(\theta^3_{SnO_2})$$

$$-k_{fwd,3\to5}.\left(\theta_{CLOSE}^{CO}\theta_{SnO_2}^{3}\right)+k_{bwd,3\to5}.\left(K_{ads,3\to5}^{CO_2}.\frac{p_{CO_2}}{R.T}\right).(\theta_{CLOSE}^{*}).(\theta_{SnO_2}^{5})$$

$$-R_{ads}^{O_2}.\theta_{SnO_2}^{3}+\frac{R_{ads}^{O_2}}{\left(K_{ads,SnO_2,3\to1}^{O_2}.\frac{p_{O_2}}{R.T}\right)}.\theta_{SnO_2}^{1}$$

$$-k_{fwd,O-transfer,3\to4}.\theta_{SnO_2}^{3}+k_{bwd,O-transfer,3\to4}.\theta_{SnO_2}^{4}$$

$$-k_{fwd,O-transfer,3\to8}.\theta_{SnO_2}^{3}+k_{bwd,O-transfer,3\to8}.\theta_{SnO_2}^{8}$$

(DV-7)

$$\frac{d\theta_{SnO_2}^{4}}{dt}=k_{fwd,2\to4}.\left(\theta_{CLOSE}^{CO}\theta_{SnO_2}^{2}\right)-k_{bwd,2\to4}.\left(K_{ads,2\to4}^{CO_2}.\frac{p_{CO_2}}{R.T}\right).(\theta_{CLOSE}^{*}).(\theta_{SnO_2}^{4})$$

$$+k_{fwd,7\to4}.\left(\theta_{CLOSE}^{CO}\theta_{SnO_2}^{7}\right)-k_{bwd,7\to4}.\left(K_{ads,7\to4}^{CO_2}.\frac{p_{CO_2}}{R.T}\right).(\theta_{CLOSE}^{*}).(\theta_{SnO_2}^{4})$$

$$-k_{fwd,4\to5}.\left(\theta_{CLOSE}^{CO}\theta_{SnO_2}^{4}\right)+k_{bwd,4\to5}.\left(K_{ads,4\to5}^{CO_2}.\frac{p_{CO_2}}{R.T}\right).(\theta_{CLOSE}^{*}).(\theta_{SnO_2}^{5})$$

$$-R_{ads}^{O_2}.\theta_{SnO_2}^{4}+\frac{R_{ads}^{O_2}}{\left(K_{ads,SnO_2,4\to1}^{O_2}.\frac{p_{O_2}}{R.T}\right)}.\theta_{SnO_2}^{1}$$

$$-k_{fwd,O-transfer,4\to3}.\theta_{SnO_2}^{4}+k_{bwd,O-transfer,4\to3}.\theta_{SnO_2}^{3}$$

$$-k_{fwd,O-transfer,4\to8}.\theta_{SnO_2}^{4}+k_{bwd,O-transfer,4\to8}.\theta_{SnO_2}^{8}$$

(DV-8)

$$\frac{d\theta_{SnO_2}^{5}}{dt}=k_{fwd,3\to5}.\left(\theta_{CLOSE}^{CO}\theta_{SnO_2}^{3}\right)-k_{bwd,3\to5}.\left(K_{ads,3\to5}^{CO_2}.\frac{p_{CO_2}}{R.T}\right).(\theta_{CLOSE}^{*}).(\theta_{SnO_2}^{5})$$

$$+k_{fwd,4\to5}.\left(\theta_{CLOSE}^{CO}\theta_{SnO_2}^{4}\right)-k_{bwd,4\to5}.\left(K_{ads,4\to5}^{CO_2}.\frac{p_{CO_2}}{R.T}\right).(\theta_{CLOSE}^{*}).(\theta_{SnO_2}^{5})$$

$$+k_{fwd,8\to5}.\left(\theta_{CLOSE}^{CO}\theta_{SnO_2}^{8}\right)-k_{bwd,8\to5}.\left(K_{ads,8\to5}^{CO_2}.\frac{p_{CO_2}}{R.T}\right).(\theta_{CLOSE}^{*}).(\theta_{SnO_2}^{5})$$

$$-R_{ads}^{O_2}.\theta_{SnO_2}^{5}+\frac{R_{ads}^{O_2}}{\left(K_{ads,SnO_2,5\to2}^{O_2}.\frac{p_{O_2}}{R.T}\right)}.\theta_{SnO_2}^{2}$$

$$-R_{ads}^{O_2}.\theta_{SnO_2}^{5}+\frac{R_{ads}^{O_2}}{\left(K_{ads,SnO_2,5\to6}^{O_2}.\frac{p_{O_2}}{R.T}\right)}.\theta_{SnO_2}^{6}$$

$$-R_{ads}^{O_2}.\theta_{SnO_2}^{5}+\frac{R_{ads}^{O_2}}{\left(K_{ads,SnO_2,5\to7}^{O_2}.\frac{p_{O_2}}{R.T}\right)}.\theta_{SnO_2}^{7}$$

(DV-9)

$$\frac{d\theta^6_{SnO_2}}{dt} = -k_{fwd,6\to3}.\left(\theta^{CO}_{CLOSE}\theta^6_{SnO_2}\right) + k_{bwd,6\to3}.\left(K^{CO_2}_{ads,6\to3}.\frac{p_{CO_2}}{R.T}\right).(\theta^*_{CLOSE}).(\theta^3_{SnO_2})$$

$$+R^{O_2}_{ads}.\theta^5_{SnO_2} - \frac{R^{O_2}_{ads}}{\left(K^{O_2}_{ads,SnO_2,5\to6}.\frac{p_{O_2}}{R.T}\right)}.\theta^6_{SnO_2}$$

$$-k_{fwd,O-transfer,6\to2}.\theta^6_{SnO_2} + k_{bwd,O-transfer,6\to2}.\theta^2_{SnO_2}$$
$$-k_{fwd,O-transfer,6\to7}.\theta^6_{SnO_2} + k_{bwd,O-transfer,6\to7}.\theta^7_{SnO_2}$$

(DV-10)

$$\frac{d\theta^7_{SnO_2}}{dt} = -k_{fwd,7\to4}.\left(\theta^{CO}_{CLOSE}\theta^7_{SnO_2}\right) + k_{bwd,7\to4}.\left(K^{CO_2}_{ads,7\to4}.\frac{p_{CO_2}}{R.T}\right).(\theta^*_{CLOSE}).(\theta^4_{SnO_2})$$

$$+R^{O_2}_{ads}.\theta^5_{SnO_2} - \frac{R^{O_2}_{ads}}{\left(K^{O_2}_{ads,SnO_2,5\to7}.\frac{p_{O_2}}{R.T}\right)}.\theta^7_{SnO_2}$$

$$-k_{fwd,O-transfer,7\to2}.\theta^7_{SnO_2} + k_{bwd,O-transfer,7\to2}.\theta^2_{SnO_2}$$
$$-k_{fwd,O-transfer,7\to6}.\theta^7_{SnO_2} + k_{bwd,O-transfer,7\to6}.\theta^6_{SnO_2}$$

(DV-11)

$$\frac{d\theta^8_{SnO_2}}{dt} = -k_{fwd,8\to5}.\left(\theta^{CO}_{CLOSE}\theta^8_{SnO_2}\right) + k_{bwd,8\to5}.\left(K^{CO_2}_{ads,8\to5}.\frac{p_{CO_2}}{R.T}\right).(\theta^*_{CLOSE}).(\theta^5_{SnO_2})$$

$$-R^{O_2}_{ads}.\theta^8_{SnO_2} + \frac{R^{O_2}_{ads}}{\left(K^{O_2}_{ads,SnO_2,8\to1}.\frac{p_{O_2}}{R.T}\right)}.\theta^1_{SnO_2}$$

$$-k_{fwd,O-transfer,8\to4}.\theta^8_{SnO_2} + k_{bwd,O-transfer,8\to4}.\theta^4_{SnO_2}$$
$$-k_{fwd,O-transfer,8\to3}.\theta^8_{SnO_2} + k_{bwd,O-transfer,8\to3}.\theta^3_{SnO_2}$$

(DV-12)

$k_{fwd,i\to j}$ is the rate coefficient of CO oxidation that borrows an oxygen atom from SnO_2 state i to yield SnO_2 state j, while $k_{bwd,i\to j}$ represents the rate coefficient of CO_2 dissociation that happens from SnO_2 state j to yield SnO_2 state i. All other parameters are very similar to the once defined above.

Remark that also the amount of SnO_2 states as well as the number oxidation reactions accounted for in the mean field micro-kinetic model has an influence on the outcome. If more oxidation reaction from SnO_2 are included, the influence of the SnO_2 is expected to be larger.

Coverage dependence of O_2 and CO desorption/adsorption

Repulsions (O -- O and CO -- CO) were included in the MF-MKM based on a spline fitting procedure on Pt(111). The same repulsions are applied on the Pt-skin system. Apart from the O—O repulsions ($\alpha(\theta^O)$) and CO—CO repulsions ($\beta(\theta^C)$), also the influence of the coverage of the other species was taken care of in cross terms ($\alpha_{\theta^O}(\theta^{CO})$ and $\beta_{\theta^{CO}}(\theta^O)$). The differential adsorption energy for O and CO was thus scaled for their coverage; with a factor $\alpha(\theta^O)$ for the oxygen, computed at different oxygen coverages as $\alpha(\theta^O) = \Delta H_{ads}^{O_2,diff}(\theta^O)/\Delta H_{ads}^{O_2}(\theta^O = 0)$. In a similar fashion, a factor $(\theta^{CO}) = \Delta H_{ads}^{CO,diff}(\theta^{CO})/\Delta H_{ads}^{CO}(\theta^{CO} = 0)$ can be computed for in function of the CO coverage.

Furthermore, cross terms were computed to estimate the effect of the coverage of CO species at $\theta^O = 1/16$; $\alpha_{\theta^O}(\theta^{CO}) = \Delta H_O^{ads}(\theta^{CO}, \theta^O = 1/16)/\Delta H_O^{ads}(\theta^{CO} = 0, \theta^O = 1/16)$, and similarly to estimate the effect of the coverage of O at $\theta^{CO} = 1/16$ ML; $\beta_{\theta^{CO}}(\theta^O) = \Delta H_{CO}^{ads}(\theta^O, \theta^{CO} = 1/16)/\Delta H_O^{ads}(\theta^O = 0, \theta^{CO} = 1/16)$.

The differential adsorption energy of a CO molecule at θ^{CO} and θ^O then becomes:

$$\Delta H_{ads}^{CO,diff,cross}(\theta^{CO}, \theta^O) = \Delta H_{ads}^{CO,\theta^{CO}=0,\theta^O=0}(\beta(\theta^{CO})\beta_{\theta^{CO}}(\theta^O))$$

Similaly, the differential adsorption energy of a O at an oxygen coverage of θ^O and a CO coverage of θ^{CO} and then becomes:

$$\Delta H_{ads}^{O_2,diff,cross} = \Delta H_{ads}^{O_2,\theta^{CO}=0,\theta^O=0}(\alpha(\theta^O)\alpha_{\theta^O}(\theta^{CO}))$$

The fitted splines (**Figures S10-S13**) are shown below:

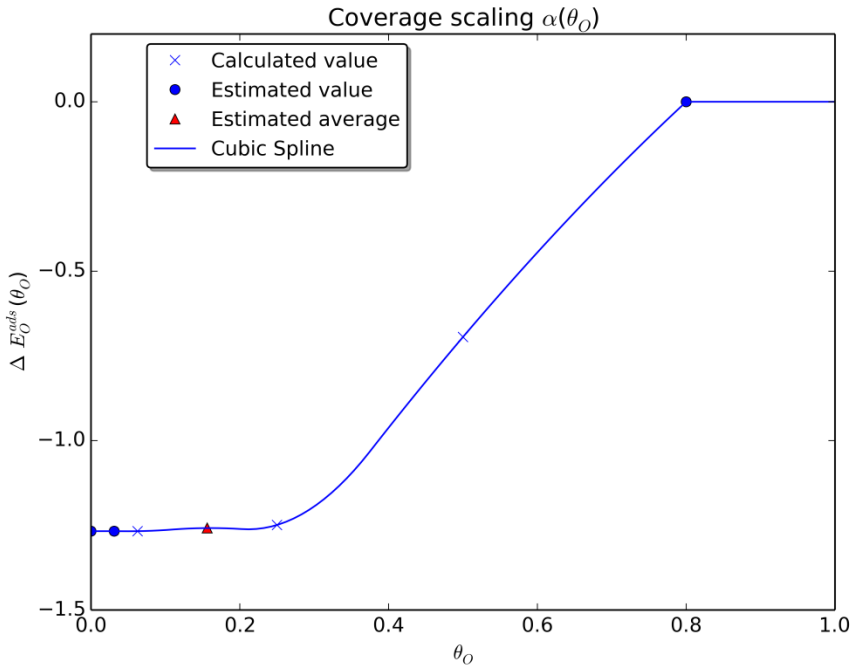

Figure S10: O-O repulsions (effect of O coverage on the O adsorption energy)

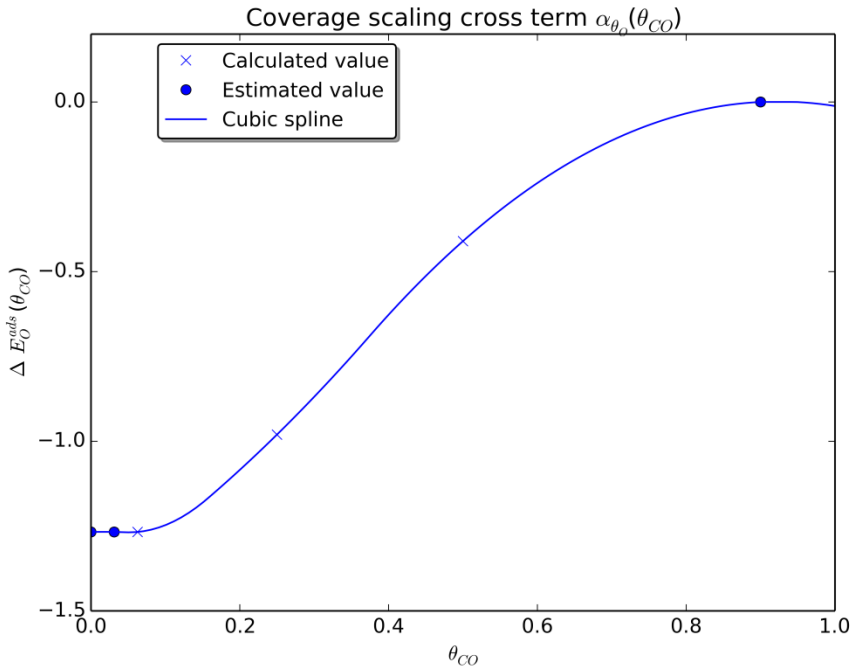

Figure S11: O-CO repulsions (effect of CO coverage on the O adsorption energy)

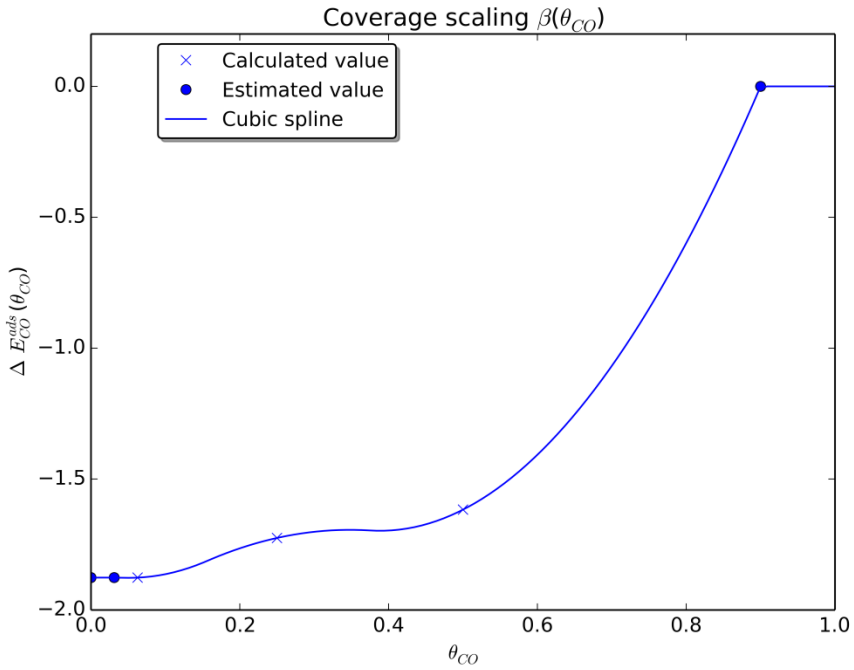

Figure S12: CO-CO repulsions (effect of CO coverage on the CO adsorption energy)

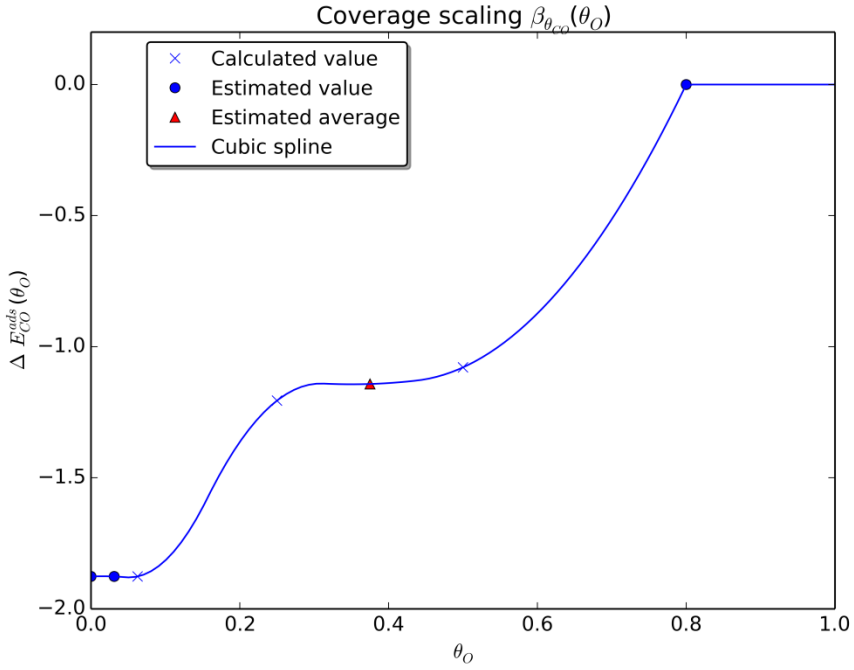

Figure S13: CO-O repulsions (effect of O coverage on CO adsorption energy)

Coverage dependence of CO oxidation barrier

Now that we can describe the adsorption of O and CO by using the proper repulsions, we can make the intrinsic barriers (from the adsorbed state of O and CO) coverage dependent. Here, we will only focus on coverage dependence of CO, since we start from a CO poisoned surface and we are interested in the light-off curve (O-coverage can be assumed low before light-off).

$$\Delta H^{\ddagger}_{Pt(111)} = \Delta H^{\ddagger,\theta^{CO}=0}_{Pt(111)} \cdot \gamma_{Pt(111)}(\theta^{CO})$$

$$\Delta H^{\ddagger}_{Pt(111)/Pt_3Sn} = \Delta H^{\ddagger,\theta^{CO}=0}_{Pt(111)/Pt_3Sn} \cdot \gamma_{Pt(111)}(\theta^{CO})$$

$$\Delta H^{\ddagger}_{interface} = \Delta H^{\ddagger,\theta^{CO}=0}_{ABC \rightarrow A*C} \cdot \gamma_{interface}(\theta^{CO})$$

The fitted splines are shown below:

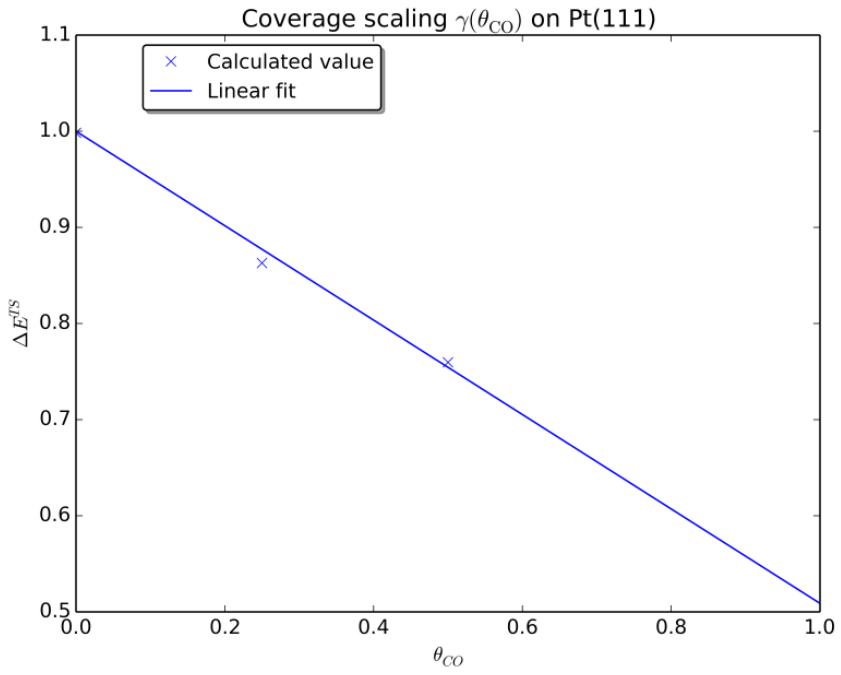

Figure S14: Effect of the CO coverage on the CO oxidation barrier on Pt(111)

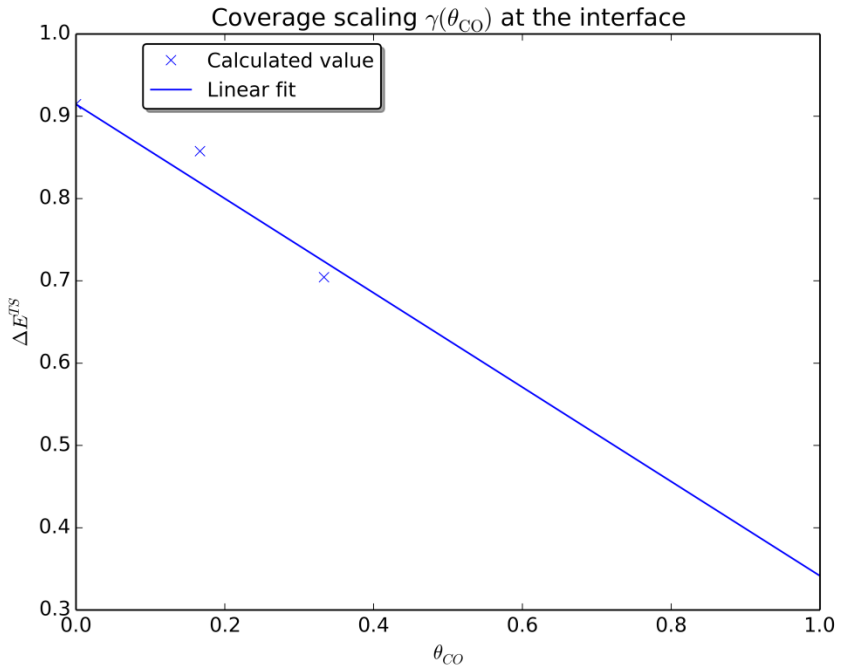

Figure S15: Effect of the CO coverage on the CO oxidation barrier at the SnO_X/Pt interface is determined for reaction ABC → A*C (see Scheme 1).

References

1. Ellner, M., *Journal of the Less Common Metals* **1981,** *78*, 21-32.
2. Reuter, K.; Scheffler, M., *Physical Review B* **2002,** *65*, 035406.
3. Jugnet, Y.; Loffreda, D.; Dupont, C.; Delbecq, F.; Ehret, E.; Aires, F.; Mun, B. S.; Akgul, F. A.; Liu, Z., *Journal of Physical Chemistry Letters* **2012,** *3*, 3707-3714.
4. Vogel, D.; Spiel, C.; Suchorski, Y.; Trinchero, A.; Schlogl, R.; Gronbeck, H.; Rupprechter, G., *Angewandte Chemie-International Edition* **2012,** *51*, 10041-10044.
5. Carlsson, P. A.; Skoglundh, M.; Thormahlen, P.; Andersson, B., *Top Catal* **2004,** *30-31*, 375-381.